

# FREQUENCY RESPONSE FUNCTIONS FOR SLIDING FRICTION CONTACTS

Christoph Kossack, John Ziegert, and Tony L. Schmitz  
Department of Mechanical Engineering and Engineering Science  
University of North Carolina at Charlotte, Charlotte, NC

## INTRODUCTION

In the study of dynamic systems, the frequency response function, or FRF, is a powerful analytical and experimental analysis tool. It defines the complex-valued frequency domain behavior, typically represented as the magnitude and phase or, alternately, the real and imaginary parts versus excitation frequency [1]. Modal testing provides a common experimental approach for identifying structural dynamics in the form of the FRF [2]. The application of impact testing, where an instrumented hammer is used to excite the structure over a sufficient bandwidth and a linear transducer is used to measure the corresponding vibratory response, is widespread in both industry and academia. While impact testing for flexible structures is commonplace, its use for measuring the dynamic response of systems with sliding contact is largely unexplored.

In this paper, an experimental platform (the friction measuring machine, or FMM) is described that enables transient, linear sliding motion between friction contact pairs under constant normal force loading [3-4]. Using the FMM, impact tests are completed with a hammer and laser vibrometer. The hammer provides the input energy in the form of a short duration impact and the system oscillates until it comes to rest (typically not at its starting position). The vibrometer measures the velocity during the decaying response as energy is dissipated in the friction contact. These experimental results are combined with simulation of a dynamic oscillator with sliding (Coulomb) friction [5] in order to parameterize idealized dynamic models that include friction.

## BACKGROUND

Friction, which can be defined as the resistance to relative sliding between two bodies in contact under a normal load [6], is ubiquitous in manufacturing, metrology, mechanical design, and control. For manufacturing processes such as forging, rolling, extrusion, drawing, sheet metal forming, machining, and grinding, friction tends to increase the required force and power; therefore, the associated cost is significant. In forging, for example, friction forces at the die-workpiece interface can cause barreling, which yields inhomogeneous deformation patterns within the workpiece. It also leads to the familiar "friction hill" pressure distribution at the die-workpiece

interface. In metal cutting, a high friction force is developed between the sheared chip and the rake face of the cutting tool in the secondary shear zone [6-10]. This, in turn, generates heat which tends to increase tool wear rates. For these and other reasons, the synthesis and testing of new lubricants and coatings to be used in manufacturing processes is an important, and continuous, research objective. Friction is also a necessary phenomenon, however. Without it, rolling, or reducing workpiece thickness using compressive forces applied by opposing rolls, would not be possible because the workpiece would not be pulled into the gap between the rolls.

Friction must also be considered in the control of manufacturing and metrology equipment. Servo-controlled, multi-axis positioning systems are widely used in: conventional and ultra-high precision machine tools; coordinate measuring machines; semi-conductor lithography equipment; micro- and nano-manufacturing systems; satellite imaging systems; and others. In many applications, axis positioning accuracies on the order of one part in  $10^6$  (or less) of the range of motion is required. For these high accuracy applications, motion velocities and accelerations are typically small, with the result that friction is often the dominant force in the system. This is true even when efforts are made to use very low friction interfaces, such as hydrostatic, aerostatic, or rolling contact bearings. Despite the use of tribological elements designed to reduce friction, it can still play a significant role in the system's positioning repeatability and accuracy [11].

Modeling and measurement of friction behavior is a critical research topic for both engineering and the physical sciences. Friction models, such as those based on adhesion or other mechanisms, relate surface condition, normal load, sliding velocity, temperature, and environment, for example, to friction forces. Traditional friction measurement attempts to assign known operating conditions, while recording the resulting friction forces. In this way, friction models may be validated (or modified) and the performance of new lubricants and coatings may be assessed. In this research, this traditional force-based (Newtonian) friction measurement paradigm is replaced by a displacement-based (Lagrangian) strategy. In prior work, the measurement uncertainty for the force-based approach was evaluated and it was

determined that its accuracy, particularly at low friction conditions, is limited [12]. This motivates the alternate Lagrangian measurement technique implemented here.

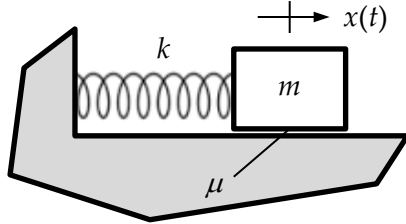


Figure 1. Spring-mass oscillator with Coulomb friction.

### SLIDING CONTACT MODEL

In this work a dynamic oscillator is used to model sliding friction (Fig. 1). When the mass is given an initial displacement from its equilibrium position, for example, this displacement characterizes the initial energy input to the system. The system is then released and allowed to oscillate until motion ceases. If the final rest position differs from the equilibrium position, energy remains in the system. During the decaying oscillation, the time dependent displacement and velocity describe the transient response. This characterizes the energy dissipation in a continuous time record. The dissipation describes the friction behavior at the interface over a range of sliding velocities from near-zero to the maximum. Alternately, the input energy can be imposed in the form of an impulsive force. Again, the system oscillates until the motion stops due to frictional energy loss.

A numerical simulation is detailed that includes an impulsive force input to initiate the oscillatory motion. The differential equation of motion is provided in Eq. 1, where  $f$  is the impulsive force input,  $m$  is the mass,  $k$  is the linear spring constant, and  $F_f$  is the friction force. For the Coulomb model, the friction force is equal to the product of the friction coefficient,  $\mu$ , and the normal force,  $N = mg$ . Given the time domain force input and corresponding response output (displacement or velocity), the FRF is determined by calculating:

1. the discrete Fourier transform of the time domain force input to convert to the frequency domain
2. the discrete Fourier transform of the time domain displacement or velocity output
3. their complex-valued, frequency domain ratio.

If displacement is selected, the receptance FRF,  $\frac{X}{F}(\omega)$ , is obtained, where  $\omega$  is the excitation frequency

in rad/s. For velocity, the mobility FRF,  $\frac{V}{F}(\omega)$ , is obtained, where  $V$  is the complex-valued velocity in the frequency domain.

$$\begin{aligned} m\ddot{x} + kx + F_f &= f, \dot{x} > 0 \\ m\ddot{x} + kx &= f, \dot{x} = 0 \\ m\ddot{x} + kx - F_f &= f, \dot{x} < 0 \end{aligned} \quad (1)$$

To demonstrate the numerical simulation, a rectangular force input with a short duration,  $\Delta t$ , was selected; its magnitude was constant over  $\Delta t$  and zero otherwise. The time domain input force and output displacement signals are presented in Fig. 2 for three  $\Delta t$  values: {2.5, 5, and 10} ms. Note the linear decay in the oscillating displacement peaks. This is indicative of friction energy dissipation and contrary to the exponential decay observed for viscous damping [5]. The corresponding receptance FRFs are shown in Fig. 3. These results demonstrate that the response changes with the amount of energy input into the system (i.e., the area under the force curve).

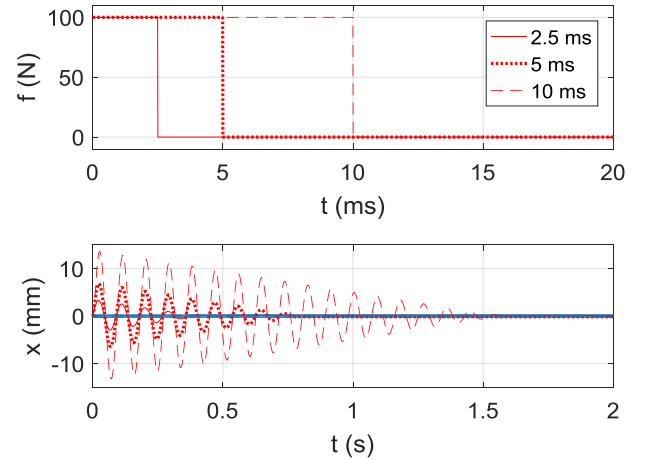


Figure 2. (Top) Impulse force input for three  $\Delta t$  values; (bottom) displacement output. Note the change in range for the time axes between the top and bottom panels.

In addition to the impulse value, changes in the friction force magnitude also modify the system response. In a second numerical study,  $F_f$  in Equation 1 was varied for a constant impulsive force input ( $\Delta t = 10$  ms with a magnitude of 100 N). In the Fig. 1 model, the normal force is fixed by the mass so the friction force can only be changed by increasing or decreasing the friction coefficient. In the experimental setup used in this research (i.e., the FMM), the normal force was set independently so this restriction was

avoided. For the purposes of this numerical examination, however, the mass was kept constant and three friction coefficients were selected:  $\mu = 0.05$ , 0.1, and 0.2. These results are displayed in Figs. 4-5.

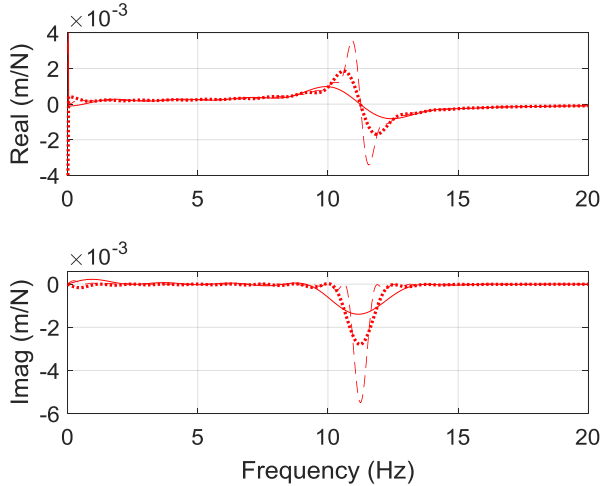


Figure 3. (Top) Real part of the receptance FRF for three  $\Delta t$  values (same legend as Fig. 2). (Bottom) Imaginary part of the receptance FRF.

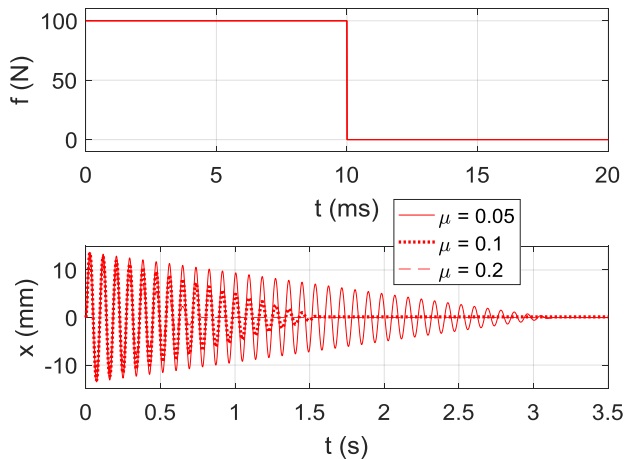


Figure 4. (Top) Impulse force input. (Bottom) Displacement output for three friction coefficient values.

### EXPERIMENTAL SETUP

The FMM provides relative linear motion between a friction contact pair (pin and flat counterface) using a parallelogram, leaf-type flexure. Figure 6 displays the four leaf spring arrangement, where one end of each spring is clamped to a rigid base and the other is clamped to a faceplate which carries the motion platform. For this study, the input energy was supplied by the hammer impact which was applied to

the motion platform at the middle of the leaf spring length to minimize platform rotation. A capacitance sensor (not shown) was used to monitor parasitic motion (i.e., arc motion perpendicular to the desired motion direction) of the platform. It was negligible when compared to the linear motion magnitude.

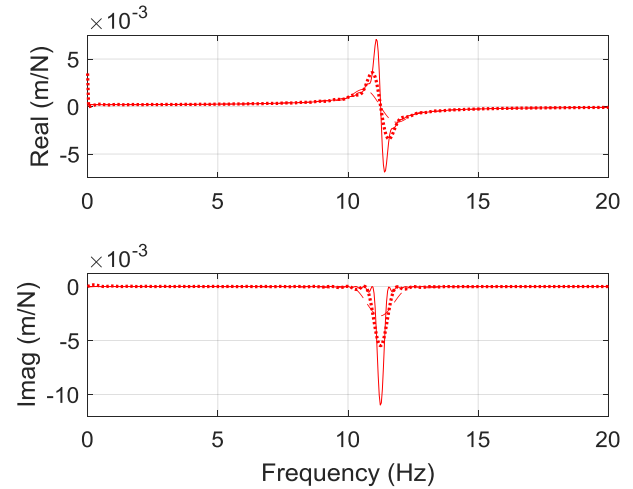


Figure 5. (Top) Real part of the receptance FRF for three friction coefficient values (same legend as Fig. 4). (Bottom) Imaginary part of the receptance FRF.

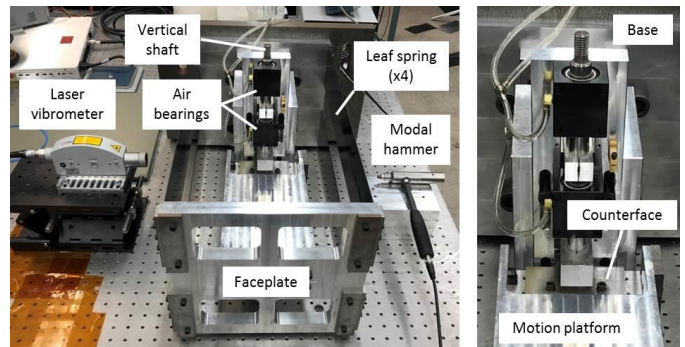


Figure 6. Photograph of FMM. They key components are identified.

The FMM dynamics with no friction contact were determined by: 1) imposing an initial displacement to the motion platform with a linear stage and electromagnet (not shown in Fig. 6); 2) measuring the corresponding free vibration velocity after release; and 3) using a nonlinear least squares optimization function in MATLAB (*lsqnonlin*) to solve for the mass, damping, and spring constants that minimized the difference between the measured velocity and the solution to the damped oscillator's second order differential equation of motion,  $m\ddot{x} + c\dot{x} + kx = 0$ , where  $c$  is the viscous damping constant that was included to account for the small energy dissipation during the flexure motion. The results were:  $m =$

10.391 kg,  $c = 0.275$  N-s/m, and  $k = 1982$  N/m. The corresponding undamped natural frequency and viscous damping ratio were:  $f_n = \frac{1}{2\pi} \sqrt{\frac{1982}{10.391}} = 2.20$  Hz and  $\zeta = \frac{c}{2\sqrt{km}} = \frac{0.275}{2\sqrt{1982(10.391)}} = 0.00096 = 0.096\%$ .

The FMM friction contact for FRF testing is produced between the pin and counterface. The pin is clamped into a holder and then attached to the vertical shaft shown in Fig. 6. The shaft is supported by a pair of air bearings, which are rigidly attached to the base. The normal force between the pin and counterface is provided by a mass attached to the top of the vertical shaft. The mass for the tests completed in this study was 0.680 kg (normal force of 6.67 N).

After the pin is clamped to the vertical shaft, it is lowered onto sandpaper which is attached by adhesive tape to the counterface. The sample is then moved back and forth for several iterations to ensure that the contacting surfaces are flat and parallel. This is repeated for a range of increasing grit numbers to leave a smooth pin face. For the tests performed here, the contact pair consisted of a polytetrafluoroethylene (PTFE) pin on a polished steel counterface. The interface was lubricated using CRC Ultra Lite 3-36 Ultra Thin Non Staining Lubricant. The lubrication was applied to ensure that each impact force level selected for testing would result in a sufficient number of oscillations during the decaying motion.

Three impact force ranges were applied to the FMM using the impact hammer. Since the impact hammer is a manual device and repeating the same force level with each impact is not possible, a tolerance of  $\pm 50$  N was selected for impact acceptance. The nominal impact force levels were 450 N (low), 1000 N (medium), and 1450 N (high). The impact force was applied using a PCB 086D05 modally tuned hammer with added mass and a rubber tip. The corresponding velocity was measured using a Polytec OFV-534 laser vibrometer head and OFV-5000 controller. The sampling time for each test was selected to be 33 s to ensure adequate frequency resolution for the FRFs. The sampling frequency was 10 kHz. The FMM was impacted by the hammer 10 times for each nominal force level. Between each impact, the CRC Ultra Lite 3-36 was reapplied to the counterface to ensure a consistent lubrication condition.

## RESULTS

The measured time domain force and velocity signals were imported into MATLAB for analysis. Figure 7 displays the impact force and velocity data for 10 trials at the medium impact level.

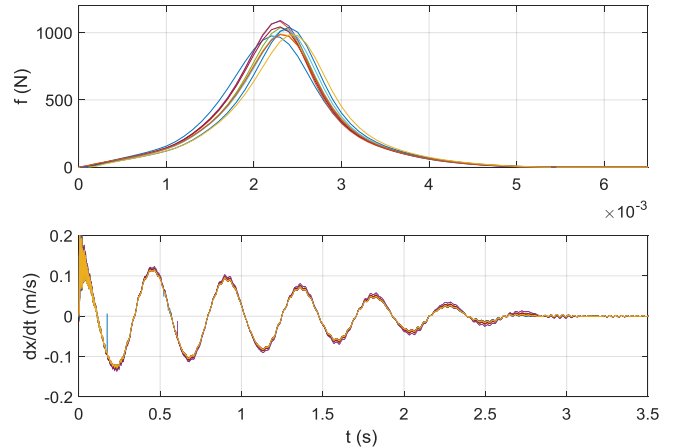


Figure 7. (Top) Time domain force,  $f$ , for 1000 N (medium) level. (Bottom) Time domain velocity,  $\dot{x}$ , due to force input. Note the change in time scale between the top and bottom panels.

The FRFs for the three force levels were determined by converting the time domain force and velocity signals into the frequency domain using the discrete Fourier transform. The mobility for each data set was then calculated by dividing the frequency domain velocity by the frequency domain force. To convert to receptance, the mobility FRF was divided by  $i\omega$ . This follows from an assumption of harmonic motion, where  $x = Xe^{i\omega t}$  and  $\dot{x} = i\omega Xe^{i\omega t}$ . Figure 8 displays the real and imaginary parts of the corresponding receptance for 10 trials at the medium force level.

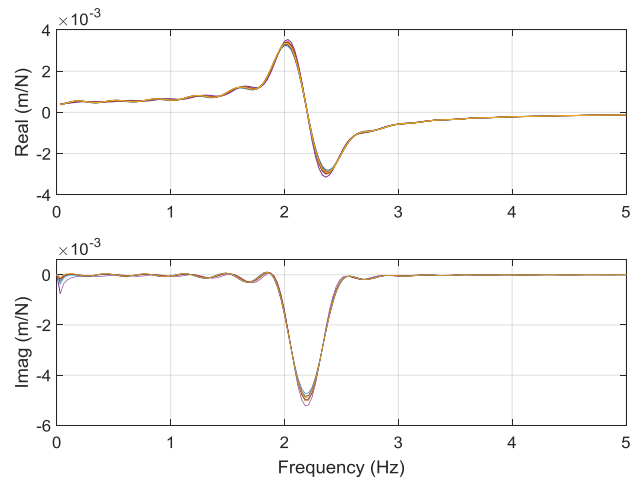


Figure 8. (Top) Real part of receptance FRF for 10 trials at the 1000 N (medium) force level. (Bottom) Imaginary part of receptance FRF for 10 trials.

The receptances are next compared for the three force levels. Figure 9 displays the mean FRF

magnitudes for the low, medium, and high levels (10 trials each, averaged in the frequency domain). Figure 10 shows the impulse versus receptance magnitude for the three force levels (mean impulse values of 0.98 N-s, 1.42 N-s and 1.64 N-s), where the + symbol identifies the mean of 10 trials at each level. A linear trend is observed with an  $R^2$  value very close to unity.

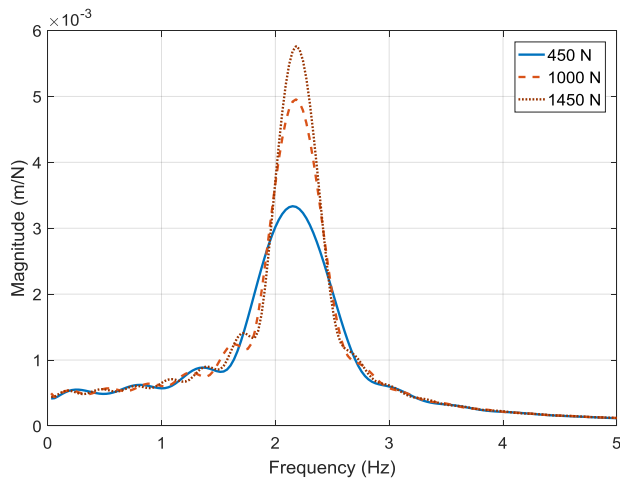


Figure 9. Mean FRF magnitude at three force levels. The magnitude increases with force for the FMM with friction contact.

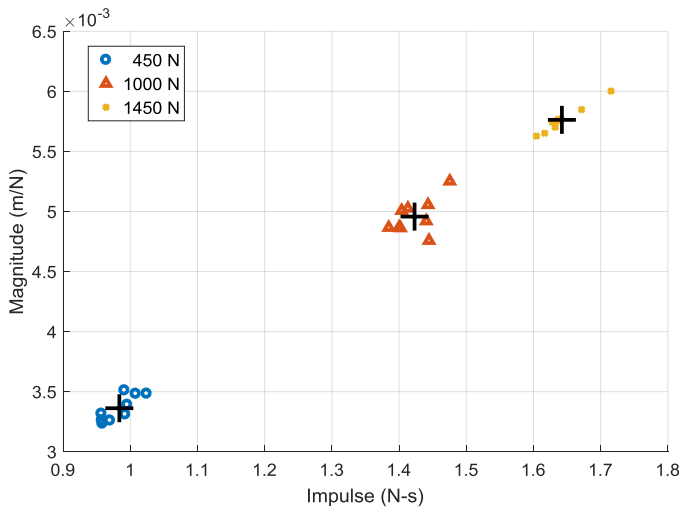


Figure 10. Impulse versus receptance magnitude for the three force levels.

Next, Eq. 1 was modified to include both sliding friction and viscous damping. This equation was solved by fixed time step numerical integration and the friction coefficient was identified to provide a best fit to the measured mobility FRFs. The measured force from the impact hammer,  $f$ , was used as input to avoid introducing errors due to approximations of

the excitation force. Because the sampling frequency for the measured force was 10 kHz, the numerical integration time step was  $1 \times 10^{-4}$  s.

A result for the 450 N (low) force level is shown in Fig. 11. The measured force is displayed in the top panel, while the simulated (solid line) and measured (dotted line) velocity are displayed in the bottom panel. The friction coefficient is 0.113. Figure 12 shows the corresponding mobility FRF. The 1000 N (medium) force levels results are provided in Figure 13. The 1450 N (high) force level results are shown in Figure 14. The friction coefficient is 0.113 in all cases.

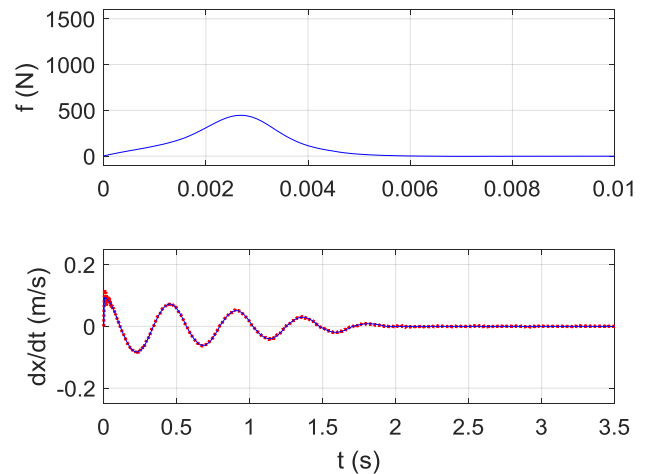


Figure 11. (Top) Low force level (450 N) input. (Bottom) Simulated (solid) and measured (dotted) velocity for 0.113 friction coefficient. Note that the top and bottom panels have different time scales.

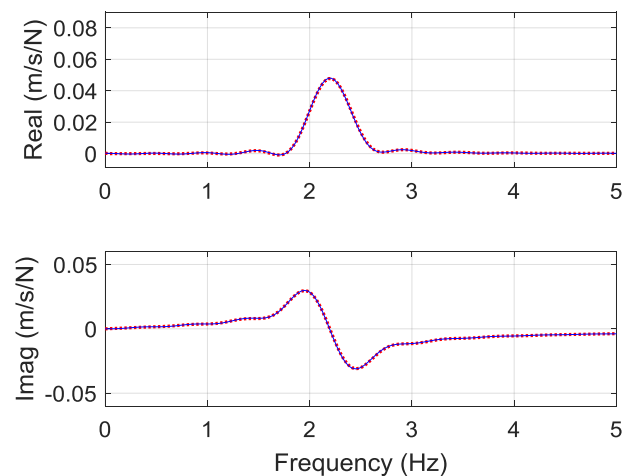


Figure 12. (Top) Real part of simulated (solid) and measured (dotted) mobility FRF for the low (450 N) force level with a friction coefficient of 0.113. (Bottom) Imaginary part of simulated and measured mobility FRFs.

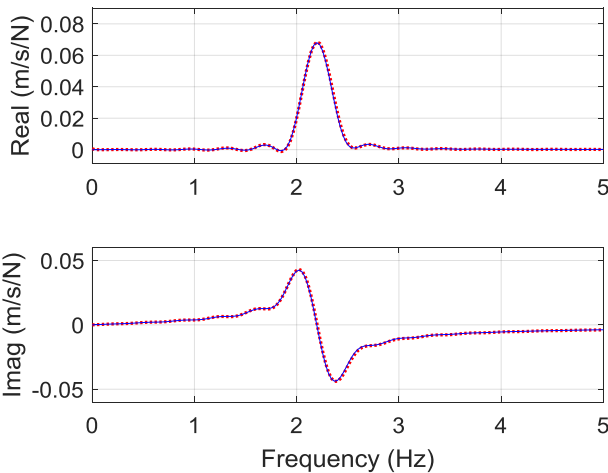


Figure 13. (Top) Real part of simulated (solid) and measured (dotted) mobility FRF for the medium (1000 N) force level with a friction coefficient of 0.113. (Bottom) Imaginary part of simulated and measured mobility FRFs.

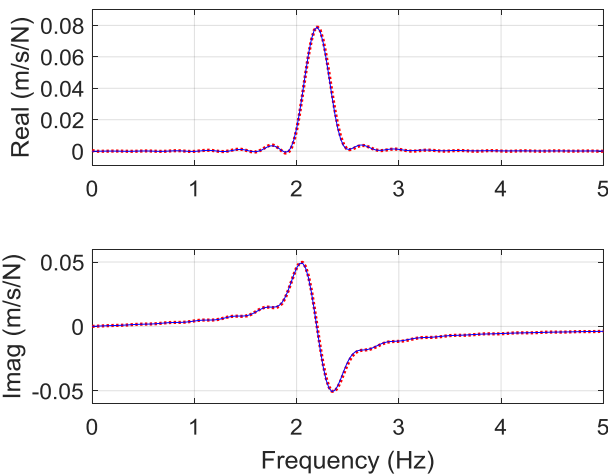


Figure 14. (Top) Real part of simulated (solid) and measured (dotted) mobility FRF for the high (1450 N) force level with a friction coefficient of 0.113. (Bottom) Imaginary part of simulated and measured mobility FRFs.

## CONCLUSIONS

This paper described frequency response function (FRF) measurement and simulation for a damped oscillator with a sliding (Coulomb) friction contact. The dynamic system was realized using the parallelogram leaf-type flexure-based friction measuring machine (FMM). The FMM enabled linear motion between a pin-counterface friction contact with impact force input. The corresponding velocity was measured to characterize the energy dissipation.

Results were presented for a lubricated polytetrafluoroethylene-polished steel contact. It was observed that the FRF magnitude increased linearly with impulse (i.e., the area under the time domain force profile). It was also seen that a single friction coefficient was sufficient to describe the response under three force levels (450 N, 1000 N, and 1450 N).

## REFERENCES

- [1] Schmitz, T. and Smith, K.S., 2012, *Mechanical Vibrations: Modeling and Measurement*, Springer, New York, NY, 2012.
- [2] Ewins, D.J., 1984, *Modal Testing: Theory and Practice*, Vol. 15, Research studies Press, Letchworth.
- [3] Lomascolo, C., Ziegert, J., and Schmitz, T., 2016, Displacement-based measurement of static and dynamic coefficients of friction, American Society for Precision Engineering Annual Meeting, October 23-28, Portland, OR.
- [4] Kossack, C., Schmitz, T., and Ziegert, J., 2017, Identification of friction energy dissipation using free vibration velocity: Measurement and modeling, American Society for Precision Engineering Annual Meeting, October 29-November 3, Charlotte, NC.
- [5] Inman, D.J., 2008, *Engineering Vibration*, Vol. 3, Prentice Hall, New Jersey.
- [6] Kalpakjian, S. and Schmid, S., 2008, *Manufacturing Processes for Engineering Materials*, 5<sup>th</sup> Ed., Prentice Hall, Upper Saddle River, NJ.
- [7] Astakhov, V., 2006, *Tribology of Metal Cutting*, Elsevier Science and Technology, Oxford, UK.
- [8] Astakhov, V., 1998, *Metal Cutting Mechanics*, CRC Press, Boca Raton, FL.
- [9] Tlusty, G., 1999, *Manufacturing Processes and Equipment*, Prentice Hall, Upper Saddle River, NJ.
- [10] Yang, X. and Liu, C.R., 2002, A new stress-based model of friction behavior in machining and its significant impact on residual stresses computed by finite element method, *International Journal of Mechanical Sciences*, 44: 703-723.
- [11] Olsson, H., Åström, K.J., Canudas de Wit, C., Gäfvert, M., and Lischinsky, P., 1998, Friction models and friction compensation, *European Journal of Control*, 4/3: 176-195.
- [12] Schmitz, T., Action, J., Ziegert, J., and Sawyer, W.G., 2005, On the difficulty at measuring low friction: Uncertainty analysis for friction coefficient measurements, *Journal of Tribology*, 127: 673-678.